FERREDOXIN-NADP$^+$ REDUCTASE FROM *Plasmodium falciparum* UNDERGOES NADP$^+$-DEPENDENT DIMERIZATION AND INACTIVATION: FUNCTIONAL AND CRYSTALLOGRAPHIC ANALYSIS

Mario Milani[1], Emanuela Balconi[2], Alessandro Aliverti[2], Eloise Mastrangelo[2], Frank Seeber[3], Martino Bolognesi[1,2], and Giuliana Zanetti[2,*]

[1]CNR-INFM, c/o Department of Biomolecular Sciences and Biotechnology, University of Milano, Via Celoria 26, 20133-Milano, Italy

[2]Department of Biomolecular Sciences and Biotechnology, University of Milano, Via Celoria 26, 20133-Milano, Italy

[3]Fachbereich Biologie/Parasitologie, Philipps-Universität Marburg, Marburg, Germany

Running title: *P. falciparum* ferredoxin-NADP$^+$ reductase structure

* Corresponding Author:
c/o Department of Biomolecular Sciences and Biotechnology
University of Milano Via Celoria 26, 20133-Milano, Italy
Fax +39 02 5031 4895
e-mail: giuliana.zanetti@unimi.it

SUMMARY

The completion of the *Plasmodium falciparum* genome sequence has recently promoted the search for new antimalarial drugs. More specifically, metabolic pathways of the apicoplast, a key organelle for survival of the parasite, have been recognized as potential targets for the development of specific new antimalarial agents. As most apicomplexan parasites, *P. falciparum* displays a plant-type ferredoxin-$NADP^+$ reductase, yielding reduced ferredoxin for essential biosynthetic pathways in the apicoplast. Here we report a molecular, kinetic and ligand binding characterization of the recombinant ferredoxin-$NADP^+$ reductase from *P. falciparum*, at the light of current data available for plant ferredoxin-$NADP^+$ reductases. In parallel with the functional characterization, we describe the crystal structures of *P. falciparum* ferredoxin-$NADP^+$ reductase in free form and in complex with 2'-phospho-AMP (at 2.4 and 2.7 Å resolution, respectively). The enzyme displays structural properties likely to be unique of plasmodial reductases. In particular, the two crystal structures highlight a covalent dimer, which relies on the oxidation of residue Cys99 in two opposing subunits, and a helix-coil transition occurs in the NADP-binding domain triggered by 2'-phospho-AMP binding. Studies in solution show that $NADP^+$, as well as 2'-phospho-AMP, promotes the formation of the disulfide-stabilized dimer. The isolated dimer is essentially inactive, but full activity is recovered upon disulfide reduction. The occurrence of residues unique to the plasmodial enzyme, and the discovery of specific conformational properties, highlights the NADP-binding domain of *P. falciparum* ferredoxin-$NADP^+$ reductase as particularly suited for the rational development of antimalarial compounds.

Keywords: ferredoxin-$NADP^+$ reductase; *Plasmodium falciparum*; apicoplast; protein structure; disulfide-stabilized dimer.

Abbreviations used: PfFNR, *Plasmodium falciparum* ferredoxin-$NADP^+$ reductase; SoFNR, *Spinacia oleracea* FNR; TgFNR, *Toxoplasma gondii* FNR; ZmFNR, *Zea mays* FNR; Fd, ferredoxin; 2'P-AMP, adenosine 2',5'-diphosphate; NMN, nicotinamide mononucleotide; DTT, dithiothreitol; INT, 2-(*p*-iodophenyl)-3-(*p*-nitrophenyl)-5-phenyltetrazolium chloride.

INTRODUCTION

The protozoan parasite *Plasmodium falciparum*, responsible for the most deadly form of malaria, causes more than 1 million deaths each year.[1] In this severe context, many drugs currently used to fight the infective disease are becoming less effective due to growing resistance displayed by the parasite in several countries, particularly in Southeast Asia. The completion of the *P. falciparum* genome sequence,[2] as well as those of other apicomplexan parasites, has promoted many efforts in the search for new drug targets and for novel antimalarial agents. Prerequisites for an ideal drug target are that the selected protein be part of a unique metabolic pathway and essential for the survival or virulence of the parasite, but ideally not present in the human host. From this point of view, apicomplexan parasites may be remarkably vulnerable since they harbor a unique organelle, the apicoplast, which is a cryptic plastid originated from the secondary endosymbiosis of a red alga.[3] This organelle has been shown to be essential for parasite survival both in *P. falciparum* and *Toxoplasma gondii*.[4,5] Thus, the metabolic pathways present or supposed to be localized in the apicoplast[6] are currently exploited as drug targets sources for the development of antimalarial agents.[7]

We have recently proposed the apicoplast redox system comprising the plant-type ferredoxin-$NADP^+$ reductase (FNR) and its substrate, the iron-sulfur protein ferredoxin (Fd), as a new potential target for design of drugs against Apicomplexa.[8] We previously reported the cloning, recombinant expression and biochemical characterization of this redox system from the apicomplexan *T. gondii*.[9-12] More recently, it was shown that the FNR/Fd pair can reconstitute *in vitro* the electron transfer pathway from NADPH to the enzyme (E)-4-hydroxy-3-methyl-but-2-enyl-diphosphate (HMBPP) reductase, also called LytB or IspH, that catalyzes the last step of the

mevalonate-independent isoprenoid biosynthesis in the apicoplast of the parasite.[13] Several other apicoplast enzymes or pathways have been suggested to be dependent on the FNR/Fd redox system, among others the iron-sulfur cluster biogenesis in the apicoplast.[8]

All apicomplexan FNRs belong to the plant-type FNR family of enzymes, for which a very detailed functional and structural characterization has been provided over the last thirty years, as summarized in recent reviews.[14-17] Up to now, the three-dimensional structure of 39 wild-type and site-directed mutant FNR forms from 6 different eukaryotic and prokaryotic sources have been deposited in the Protein Data Bank, some of which are FNR complexes with either of the two substrates, Fd or NADP(H).

In our continuous effort to understand the functional and structural aspects of plant FNRs but also to lay the foundations for exploiting apicomplexan FNRs as drug targets, we report here the basic biochemical characterization and three-dimensional structure of *P. falciparum* FNR (PfFNR) in two different crystal forms, in the absence and presence of the nucleotide analogue adenosine 2',5'-diphosphate (2'P-AMP). We show that PfFNR undergoes a dimerization process that is dependent on the redox conditions and on the presence of $NADP^+$ or 2'P-AMP, leading to a virtually inactive homodimeric enzyme. The structural data also show that conformational disorder affects protein loops that are specific of the apicomplexan parasite reductase, while conformational transitions at the 2'P-AMP site may promote formation of the dimeric species. Altogether, the data presented here shed first light on the functional and structural properties of a protozoan FNR, providing a rational basis for the design of inhibitors that might be developed into antimalarial drugs.

RESULTS

a) Molecular and kinetic characterization of PfFNR – The absorbance spectrum of the purified recombinant PfFNR in the visible region is that typical of this flavoprotein family, with peaks at 394 and 454 nm, and a A_{280}/A_{454} ratio of 7.0. The presence of a modified flavin, as reported for the recombinant form of *T. gondii* apicomplexan FNR that contains variable amounts of 6OH-FAD,[18] could thus be excluded. An extinction coefficient of 10 mM^{-1} cm^{-1} (at 454 nm) was determined and used throughout for enzyme quantification. Being devoid of Trp residues, PfFNR displays very low protein fluorescence, and the FAD fluorescence is nearly fully quenched.

PfFNR was homogeneous by SDS-PAGE analysis, and had an electrophoretic mobility consistent with the calculated theoretical mass of 37,267 Da. PfFNR was shown to be a monomer of 28 ± 1.4 kDa by gel filtration on a Superdex 75 column in FPLC. Following the crystallization results (see below) that indicated the presence of a disulfide-stabilized PfFNR dimer in both crystal forms analyzed, the six Cys residues of the enzyme were titrated with DTNB, both under native and denaturing conditions. These experiments revealed that only one Cys could be titrated in the native protein, and practically all Cys residues (5.45) were modified in the denatured enzyme. To further proof that the PfFNR intermolecular disulfide was the result of Cys oxidation occurring during crystal growth (*i.e.*, on a long exposure to air) two protein samples were incubated at 20 °C in the presence and absence of 1 mM DTT, respectively. Aliquots were withdrawn at different times and gel-filtered on the Superdex 75 column, as described above (see Fig. 1A). After about seven days of aerobic incubation, a peak eluting in front of that corresponding to the PfFNR monomer was observed in the DTT-free sample. The molecular mass of this species was 44 ± 2 kDa, compatible with that expected for a PfFNR

dimer. The dimer peak grew in intensity with time, and was also observed in the aged sample containing 1 mM DTT. After addition of fresh DTT to both aged samples, gel-filtration showed only one protein peak corresponding to the monomeric species (data not shown).

Taken together, these data indicate that formation of a disulfide-stabilized PfFNR dimer is related to spontaneous air oxidation occurring during the relatively long time needed for the growth of PfFNR crystals. The above experiments were repeated including 1 mM 2P'-AMP in the aerobic incubation mixtures. As shown in Fig. 1B, just after 1 h of incubation under these conditions, the dimer was detectable, its amount increasing rapidly to 37% after 1 day, and to 73% after 4 days. Activity measurements after 4 days of incubation indicated that the mixture containing more than 70% of dimer was much less active (*ca.* 20%) than a control sample incubated for the same time. To evaluate whether formation of the dimer has any significance *in vivo*, $NADP^+$ was used instead of 2P'-AMP in the incubation mixture. Indeed, as shown in Figure 1C, $NADP^+$ as well is able to promote dimer formation with concomitant decrease of activity. Furthermore, dimer formation was studied with enzyme and coenzyme at more physiological concentrations by measuring residual activity. 4 μM PfFNR incubated with 200 μM $NADP^+$ yielded nearly the same amount of dimer, *i.e.*, 10% at 1 h and 50% at 24 h *versus* 12% and 49%, respectively (at 300 μM PfFNR, 1 mM $NADP^+$, Fig. 1C). In all the above experiments, addition of 1 mM DTT completely dissociated the dimer and fully restored PfFNR enzymatic activity.

The NADPH–$K_3Fe(CN)_6$ diaphorase reaction is typically used to kinetically characterize FNR enzymes, because of the simplicity of the assay and due to the fact that the reaction rate was shown to be limited by FAD reduction in the case of FNR from spinach leaves (SoFNR).[19]

At 1 mM ferricyanide and varying the NADPH concentration, an apparent k_{cat} value of 214 s^{-1} was determined for PfFNR, with a K_m for NADPH of 172 μM. These values deviate significantly from those found for plant and *T. gondii* FNRs,[10,19,20] the PfFNR activity being lower and K_m for NADPH remarkably higher. By varying the concentration of the diaphorase reaction acceptor, a pattern became evident (*i.e.*, rates increased upon decreasing the ferricyanide concentration) that could be fitted by an equation that considers ferricyanide acting as a competitive inhibitor of NADPH (K_i of 230 μM). This analysis yielded nearly the same k_{cat} value reported above, while the apparent K_m for NADPH was found substantially lower (Table 2). NADH was also tested as a possible electron donor in the ferricyanide reduction, but it turned out to be a poor substrate. The ratio of the specificity constants (k_{cat}/K_m^{NADPH} divided by k_{cat}/K_m^{NADH}) yielded a value of 70 indicating a much lower capacity of PfFNR to discriminate between the two pyridine nucleotides relative to the plant enzymes (specificity constant ratios ≥ 30,000).

The kinetic parameters were also determined for the PfFNR homodimeric species. The PfFNR dimer produced after 36 h of aerobic incubation in the presence of 1 mM $NADP^+$ was isolated by gel-filtration as described above. The dimer exhibited the same spectral ratio A_{280}/A_{454} as the monomeric species. The k_{cat} value turned out to be only 5% of that of monomeric PfFNR, while the K_m for NADPH was of the same order (*ca*. 23 μM; see Table 2). An alternative electron acceptor for FNRs is INT. As shown in Table 2, the values of the kinetic parameters for this reaction fall in the range observed for the other FNRs, except for the very high value of K_m for NADPH. Using the INT assay, a K_i of 134 ± 14 μM (versus an apparent K_m

for NADPH of 232 ± 15 μM) for 2'P-AMP, a typical competitive inhibitor of NADPH-dependent enzymes, was measured.

b) $K_3Fe(CN)_6$, 2'P-AMP and $NADP^+$ binding – The difference spectrum in the visible region resulting from $NADP^+$ binding to PfFNR showed, besides the positive peak at 508 nm, a second lower positive maximum at 475 nm, which in SoFNR-$NADP^+$ complex difference spectrum is a small shoulder[20,21] (Fig. 2A). Titrations of the enzyme at pH 7 with increasing concentrations of $NADP^+$ allowed us to determine a K_d value of 35 ± 7 μM (vs 14 μM for SoFNR),[21] which indicates a low affinity of PfFNR for the oxidized pyridine nucleotide. Titration of PfFNR with 2'P-AMP yielded a canonical difference spectrum for the FNR enzymes[21] (Fig. 2A), and a K_d value of 2.4 ± 1 μM (the same value of SoFNR).[21] Since $K_3Fe(CN)_6$ was found to inhibit PfFNR, its interaction with the enzyme was also studied by difference spectroscopy. Addition of the dye to the oxidized enzyme also elicited spectral perturbations of PfFNR, resulting in a difference spectrum similar to that of the 2'P-AMP complex but with distinct features (Fig. 2A). The approximate value determined for K_d was in the same range as that found for K_i. To evaluate if competition for the same site (or overlap of the binding sites) between ferricyanide and 2'P-AMP takes place, titrations of the 2'P-AMP–enzyme complex with ferricyanide and *viceversa* were performed. Clearly, the two difference spectra were additive, excluding the binding of ferricyanide at the same site of 2'P-AMP. Similar experiments were performed with ferricyanide and $NADP^+$. Titration of the $NADP^+$-enzyme complex with $K_3Fe(CN)_6$ perturbed its difference spectrum producing a progressive decrease of the peak at 510 nm (which is typical for the $NADP^+$-enzyme complex) with the concomitant appearance of the difference spectrum of the

ferricyanide-enzyme complex (Fig. 2B). This suggests that ferricyanide competes with the NMN part of $NADP^+$ for binding to the PfFNR active site.

c) Overall structural properties of PfFNR – The two crystal forms of PfFNR reported here were obtained in the absence of 2'P-AMP ($P3_221$ space group crystals) and in its presence ($P3_1$ space group crystals), respectively. As expected for this enzyme family,[14] PfFNR consists of two domains: the N-terminal FAD binding domain, comprising residues 1 - 160, and the C-terminal $NADP^+$ binding domain, built by residues 166 - 316 (Fig. 3A, B). Accordingly, the FAD domain hosts a β-barrel built by two perpendicular three-stranded antiparallel beta sheets (β1β2β5 and β3β4β6) and a single α-helix (αA), nestled between β5 and β6. The C-terminal domain hosts a five-stranded parallel β-sheet (β9β8β7β10β11), surrounded by seven α-helices (αB-αH). In both crystal forms PfFNR displays five disordered surface regions: the N-terminal residues 1-4, the long loop between β3 and β4 (residues 63-97), the β5-αA loop (residues 126-133), the αB-β9 loop (residues 196-205), and the αH-αI (residue 299-305). Excluding such regions, the r.m.s. deviations calculated on 244 Cα atoms for the six independent protein chains (of the PfFNR/2'P-AMP inhibitor complex, PfFNR/2'P-AMP) range between 0.30 and 0.58 Å, the main structural differences being located at the borders with the disordered regions. Structural comparisons with maize root FNR (ZmFNR, pdb id. 1JB9; 29% sequence identity) and SoFNR (pdb id. 1FND; 25% sequence identity) yield r.m.s. deviations of 1.61 Å (234 Cα pairs) and 1.70 Å (237 Cα pairs), respectively. Slightly lower r.m.s. deviation values (about 1.5 Å) result from structural overlays of PfFNR in the absence of 2'P-AMP ($P3_221$ crystal form) with the same two plant enzymes.

d) The FAD binding site – The FAD molecule is observed essentially in the same extended conformation in both crystal forms. The 7,8-dimethyl-isoalloxazine ring is hosted in a pocket between the two protein domains, sandwiched between the conserved C-terminal Tyr316 and four conserved amino acids of the β4 strand. The FAD adenine end points toward the protein surface, where slight orientation differences (about 1.5 Å) are observed in the two crystal forms (Fig. 3A, B). Schematically, the FAD molecule interacts with four main regions of PfFNR, largely through hydrogen bonds to/from atoms of the main chain. These regions comprise the strands β4 (Arg101 NH2, Leu102 O, Ser104 N atoms) and β5 (Ala117 O, Lys119 N, Tyr123 O atoms), the αA helix (Tyr137 N, Cys138 N, Ser139 Oγ atoms), and the conserved C-terminal Tyr316 at the end of strand β11. Two water molecules (w1 and w2) mediate interactions between the protein and the dimethyl-isoalloxazine ring through hydrogen bonds to its carbonyl oxygen atoms (O2 and O4): w1 bridges between His121 Nε2, Lys119 O, the ribitol hydroxyl O3 and O2, whereas w2 bridges between Ser104 O, Ala 117 atoms O and N, and the isoalloxazine carbonyl oxygen O4. The ribitol hydroxyl O3 is also hydrogen bonded to Tyr103 OH, whereas the FAD diphosphate moiety interacts with the N atom of Cys138, and with the N and O γ atoms of Ser139, the negative charges being partly compensated by Arg101. Finally, the adenine ring stacks over the phenolic ring of Tyr123.

The overall FAD binding mode described for PfFNR is essentially conserved in ZmFNR and SoFNR, the main conformational differences affecting only the protein surface location of the cofactor's adenosine moiety (displaced by 1.7 Å in ZmFNR and by 5 Å in SoFNR). Such surface location accounts for the (contained) mobility of the FAD adenosine end observed in two

crystal forms of PfFNR and in ZmFNR. Due to a varied disposition of the β5-αA loop, the FAD adenosine end is further projected towards the solvent in SoFNR, where it is also differently oriented, being stabilized only by a stacking interaction with Tyr120. The enhanced mobility of the adenine ring is stressed by considering the ratio of B factors between adenine atoms and atoms of the isoalloxazine ring within the FAD cofactor of different enzymes. This ratio is about 2.5 for ZmFNR and PfFNR, but it is 11.8 in SoFNR. Given the location of the FAD adenine ring far from the active site region, such structural variations should bear little relevance for PfFNR catalysis.

e) PfFNR structure in the absence of 2'P-AMP – The $P3_221$ PfFNR crystals accommodate four molecules in the asymmetric unit; the crystal lattice packing gives rise to an open tetramer with approximate 222 symmetry (Fig. 3C). Within such a tetramer, covalent dimers based on an intermolecular disulfide bridge involving Cys99 (in the FAD binding domain) from facing PfFNR subunits can be recognized in the crystal structure (Fig. 3D). Two distinct association interfaces can be recognized in such tetrameric assembly. The first intermolecular association interface in the region surrounding the Cys99 disulfide covers 720 $Å^2$. Such a contact region occurs in a part of the FAD binding domain that is characterized by disordered loops. The covalent dimeric association locates two FAD groups about 18 Å apart (closest approach) in anti-parallel fashion. The second association interface (supporting non-covalent protomer association in the tetramer, via a local 2-fold axis) covers 460 $Å^2$, and is built by helices αF and αH of opposing protomers, related by a local 2-fold axis. The FAD groups related by this association

interface fall 37 Å apart. Cα backbone superposition of 258 model built residues in the four PfFNR chains yields r.m.s.d. values in the 0.51 - 0.57 Å range.

f) PfFNR/2'P-AMP complex structure – PfFNR/2'P-AMP crystallizes in the trigonal $P3_1$ space group, with six asymmetric unit complex moieties that are assembled into three evident dimers. Comparison with the enzyme structure reported above shows that 241 Cα atoms of PfFNR/2'P-AMP match the PfFNR protein backbone with a r.m.s.d. of 0.80 Å. Association of the dimeric assembly relies on a contact surface of about 1420 $Å^2$ on each protomer, being stabilized by the intermolecular Cys99-Cys99' disulfide bridge reported above for the inhibitor-free protein (Fig. 3E). Nevertheless, the dimeric PfFNR assembly achieved in the 2'P-AMP complex is essentially unrelated to that observed in the absence of the inhibitor. The two PfFNR protomers in PfFNR/2'P-AMP contact each other mostly through the active site surface, in such a way that parts of the FAD binding domains of the two protomers (and of the $NADP^+$ binding domains as well) face each other, in a quaternary assembly displaying approximate 2-fold symmetry (Fig. 3E). The association gives rise to a sort of central tunnel (open diameter of 6-7 Å), orthogonal to the dimer's 2-fold axis, defined by the four domains in the two protomers. The tunnel walls are lined by two FAD and two 2'P-AMP molecules. Water molecules are found at several different locations, mediating interactions at the dimer association interface. In each dimer two FAD molecules assemble in antiparallel fashion around the local 2-fold axis; the 7- and 8-methyl groups of one isoalloxazine ring contact (3.5 – 3.9 Å) one face of the adenine ring of the opposing FAD moiety. Additionally, two water molecules bridge between the ribitol O4 atoms of the two facing FAD molecules. Direct hydrogen bonding interactions are observed in the

$NADP^+$ binding domain between the 2'P-AMP molecules of opposing protomers (see Section *g*) below). Electrostatic compensation between residues and the inhibitor and direct hydrogen bonds between residues of the two facing protomers can be distinguished in this subset of the association interface.

g) The 2'P-AMP binding site – The 2'P-AMP molecule is located in a cleft at the C-terminal end of the core β sheet, in the $NADP^+$ binding domain, as expected. The inhibitor interacts mostly with two regions: β9-αF (hydrogen bonds to Ser247 Oγ, Tyr258 OH, Gln260 Oε1 atoms), and β10-αH (hydrogen bonds to His286 Nε2, Ser288 Oγ atoms) of the C-terminal domain, and with Lys119 Nζ of the N-terminal domain. The negative charge of the 5' phosphate is balanced by Lys119, by a putative sodium ion, and by His286, whereas the negative charge of 2' phosphate can be compensated only by Lys287 and/or Lys292, both contributed from the opposing subunit in the dimeric assembly (Fig. 4). Moreover, the inhibitor's 2' phosphate is hydrogen bonded to the conserved residues Ser247 and Tyr258, and to Ser288 (the latter from the facing PfFNR subunit). Such series of interactions suggests that the achievement of inter-molecular electrostatic balance at the 2' phosphate might be one of the driving forces guiding PfFNR dimerization induced by 2'P-AMP or by $NADP^+$.

The 2'P-AMP adenine moiety is stabilized by three hydrogen bonds: two connecting to the 2'-AMP adenine ring of the facing subunit (atoms N6 and N7, in a reversed Hogsteen A-A base pairing), and the third to Ser288 Oγ. The adenine is sandwiched between Tyr258 and His286, and parallel to both side chain rings, in a position matching that of 2'P-AMP in its complex with SoFNR,[22] where the 2' phosphate charge, however, is compensated intra-

molecularly by the highly conserved residues Arg235 (Tyr248 in PfFNR) and Lys244 (Ser256 in PfFNR). Indeed, despite the sequence differences and the conformational transitions occurring at residues 248-257 and 289-298 of PfFNR upon binding of 2'P-AMP (described in Section *h*)), the inhibitor binding mode appears essentially the same in the two enzymes, with 3 Å deviations in the position of the 5' phosphate end. Finally, it should be noted that the locations of the adenine stacking residues Tyr258 and His286 (a PfFNR specific residue) are dictated in PfFNR/2'P-AMP by their interactions with the inhibitor 2' and 5' phosphate groups, described above.

The observed PfFNR/2'P-AMP crystal structure allows to draw some hypotheses on the binding mode of $NADP^+$ to PfFNR. We model built a $NADP^+$ molecule in PfFNR by transfer of the nucleotide structure from the 3D structure of the homologous $NADP^+$ bound *Pisum sativum* FNR (bearing the Tyr308Ser mutation; PDB entry 1QFY) after proper structure superposition (r.m.s.d deviation between the two protein backbones of 1.69 Å, for 239 Cα pairs). Inspection of the built PfFNR/$NADP^+$ model indicates that both the 2' and 5' phosphate groups may keep the same disposition in the two enzymes, the 5' phosphate falling next to the conserved residue Lys119. The nicotinamide ring can be easily fitted next to the FAD isoalloxazine ring, replacing the stacking interaction of Tyr316, potentially being stabilized by a hydrogen bond to the conserved residue Glu314. The $NADP^+$ adenosine end matches closely the 2'P-AMP binding mode in this PfFNR region. However, as described above, electrostatic balance of the 2'-phosphate (occurring with the two conserved residues Arg235 and Lys244 in SoFNR) is missing in PfFNR (where these residues are Tyr248 and Ser256). Such deficiency of electrostatic compensation, as described above for 2'P-AMP, could promote dimerization of

PfFNR/$NADP^+$ via the interaction of the 2' phosphate with residue Lys287 from the facing subunit (Fig. 4).

h) Conformational transitions related to 2'P-AMP binding – The most striking differences evident from the structural comparison of PfFNR/2'P-AMP and PfFNR are located in the $NADP^+$ binding domain; they involve the β9-αF loop (residues 248-257) and the αH helix (residues 289-298). In fact, in the absence of the inhibitor a hydrogen bonded salt bridge formed by His286 and the 2'P-AMP 5' phosphate is severed, and the nearby αH helix is shifted towards the FAD binding pocket by about 2 Å. Concomitantly, the β9-αF loop is shortened by 7 residues relative to PfFNR/2'P-AMP, and the αF helix is elongated by two additional turns at its N-terminus (residues Ser252-Tyr258) (Fig. 3A). Such conformational transition linked to binding of 2'P-AMP and affecting the β9-αF and αH regions (but also the αH-β11 loop, which is disordered in the PfFNR/2'P-AMP structure) has not been observed before in any FNR, and is also reflected by a hydrogen bond stabilizing the β9-αF short loop in the inhibitor-free enzyme (Fig. 3A). If 2'P-AMP were to bind to the PfFNR observed structure, the inhibitor adenosine 2' phosphate moiety would collide with the amino acid region comprised between Lys249 and Ser256, whereas the 5' phosphate would be in close contact with Ser252, thus explaining the large conformational readjustments affecting the β9-αF loop described above for PfFNR/2'P-AMP (Fig. 3A).

DISCUSSION

Amino acid sequence comparisons of PfFNR relative to plant, algal and plasmodial FNRs show that out of the four conserved Cys residues in the FNR family (*i.e.* Cys114, Cys132, Cys137 and Cys272, SoFNR numbering), only Cys132 and Cys272 are present in PfFNR, which however displays a total of six cysteines.[9,23] As most apicomplexan enzymes, PfFNR contains two major sequence insertions of 28 and 5 amino acids, respectively. The longer insertion falls just before the FAD binding motif and the shorter is a few amino acids after the $NADP^+$ binding GTG sequence motif. The first inserted segment is reflected by a disordered loop in both PfFNR and PfFNR/2'P-AMP structures, covering residues 62-96, after which the polypeptide chain returns to a defined conformation, also in consideration of the neighbouring Cys99 disulfide bridge. The 5-residue insertion occurs in a wide surface loop, also displaying conformational flexibility that hampers the observation of residues Asp196-Ser205 in the αB-β9 loop. These structural results are in full agreement with the data obtained by limited proteolysis on TgFNR.[12] Indeed, most of the protease cleavage sites identified in TgFNR fall in these sequence insertion segments.

Several sequence differences, relative to plant FNRs, are present in the FAD and in the $NADP^+$ binding motifs, which are otherwise highly conserved within the FNR family (Fig. 5). Among these the lack of two basic residues (Arg235 and Lys244) which have been shown to stabilize the 2'P of $NADP^+$ and of 2'P-AMP in SoFNR[22,24,25] is remarkable. This could explain the observed lower affinity for NADPH and $NADP^+$ shown by PfFNR in comparison to other FNRs. The specific electrostatic features of the NADP(H)-binding site could result in subtle differences in the geometry of bound NADPH, causing the lower k_{cat} value of the plasmodial enzyme in the NADPH-ferricyanide reductase reaction.

The structural results reported here highlight the unexpected role of Cys99, a residue conserved (although not fully) in plasmodial FNRs; conversely, this site is never occupied by Cys in plant FNRs. PfFNR Cys99 acts specifically in the formation of an intermolecular disulfide bridge resulting in the enzyme association into dimers. The high reactivity displayed by Cys99 may be related to its full solvent accessibility, but also to the nearby location of positively charged residues, such as Lys13, Arg98 and Arg101, that may increase the residue's reactivity by enhancing its nucleophilic character. The crystallographic results show that binding of 2'P-AMP to PfFNR promotes formation of a compact dimer, whose subunit association interface is properly shaped by the enzyme interaction with the inhibitor. Such interaction requires a substantial restructuring of 12 residues in the β9 – αF region (undergoing a helix-coil transition for residues Asn251 – Phe257), and a 2 Å shift for the αH helix. It is remarkable that, despite the unique sequence displayed by PfFNR, the elongated αF helical structure seen in this region of inhibitor-free PfFNR changes into one that is topologically much closer to ZmFNR and SoFNR, showing a shorter αF helix and a longer β9 – αF solvent exposed loop.

The dimeric assembly observed in 2'P-AMP-free PfFNR might represent a resting state of PfFNR, once the Cys99 disulfide is formed. Inspection of the 3D structures indicates that the inhibitor-free PfFNR assembly cannot give rise to the quaternary structure of PfFNR/2'P-AMP for two main reasons. On one hand, the extended α-F helix alters the subunit association interface and would yield intermolecular collisions at the 2'P-AMP binding sites. On the other, the (electrostatic) intermolecular interactions established by the inhibitor and the opposing enzyme subunit are obviously missing. None of the structural data, however, helps in assessing whether the observed dimeric form has a functional role within the apicoplast, where specific

(yet uncharacterized) redox properties may prove crucial in promoting/preventing formation of the dimer-stabilizing disulfide bridge.

Our results show that in dimeric PfFNR/2'P-AMP the inhibitor 2' phosphate may be counterbalanced by the positive charges of Lys287 and/or Lys292 of the facing subunit, being stabilized by intra- and intermolecular hydrogen bonds. The crystal structure of PfFNR/2'P-AMP shows that His286, that appears to be unique to the PfFNR sequence, contributes substantially to stabilization of the 2'P-AMP inhibitor, since it is stacking over the adenine aromatic ring (the other stacking partner on the opposite adenine face being Tyr258) and it is hydrogen bonded to the inhibitor 5' phosphate. At the crystallization pH of 6.0 the His286 – 2' phosphate interaction is likely to display also a strong ion pair character. This residue is part of a loop (residues 284-291) proposed to be involved in NAD(P)(H) recognition and to represent one of the determinants of coenzyme specificity within the FNR superfamily.[26] Indeed, it has been shown by site-directed mutagenesis that Leu263 of *Anabaena* FNR, equivalent to His286 of PfFNR, plays a significant role in NADPH binding and discrimination against NADH,[27] though it provides only a modest apolar contact to the adenine ring of the ligand.[22,28]

From the functional viewpoint the ability of PfFNR to undergo a redox-linked inactivation/reactivation process based on a disulfide/dithiol interchange at Cys99 is so far unique in the FNR family. As shown by the crystal structures and the gel filtration experiments, the observed active and inactive forms of PfFNR correspond to its monomeric and disulfide-stabilized dimeric states, respectively. Thus, the results here reported allow us to rationalize on a molecular basis the very low catalytic activity of the disulfide-linked homodimeric form of the enzyme. Indeed, the 2'P-AMP-bound form of dimeric PfFNR adopts a very compact quaternary

structure, where both NADP- and Fd-binding sites are poorly accessible. It can be speculated that during the catalytic cycle the dimeric form of PfFNR stalls in a conformation similar to that observed for the PfFNR/2'P-AMP complex, where 2'P-AMP would be replaced by $NADP^+$. Under these conditions, both $NADP^+$ release and electron transfer from $FADH_2$ to the acceptor substrate should be impaired, justifying the low k_{cat} value displayed by the PfFNR dimer in the ferricyanide reductase activity.

The comparison of two crystal forms of PfFNR additionally suggests a mechanism explaining the onset of enzyme inactivation triggered by $NADP^+$ or its analog. We hypothesize that the active, free-thiol form of PfFNR can exist in solution as an equilibrium mixture of monomer and non-covalent homodimer. When $NADP^+$ (or its analog) is bound, the PfFNR dimer is expected to match closely the quaternary structure of the PfFNR/2'P-AMP complex observed in the crystals, which is stabilized by a relatively wide subunit interface involving the bound ligand. Conversely, in the absence of $NADP^+$, the non-covalent (dimer forming) interactions are destabilized due to partial reorganization of the C-terminal domain and to the lack of the bridging contacts provided by the ligand. The presence of $NADP^+$ would therefore drive the monomer-dimer equilibrium towards subunit association, while in the absence of $NADP^+$, PfFNR dimers would hardly be present. The close proximity of two Cys99 β-SH groups from facing subunits in the PfFNR non-covalent dimer would promote thiol oxidation to disulfide, and covalent stabilization of the dimer.

The observed rate of Cys99 disulfide formation is relatively low when O_2 is the oxidant species. The rates of dithiol/disulfide interconversion are expected to be substantially higher *in vivo*, where the process can be speeded up by appropriate catalysis. It is noteworthy in this

respect that when oxidants other than oxygen (*e.g.*, diamide) are used, the disulfide-linked dimer is formed *in vitro* at much higher rates (data not shown). Redox regulation of enzymes through disulfide bond formation is a common theme in plant metabolism. In addition to the well known examples described in chloroplasts, similar regulatory mechanisms have been recently observed in plant non-photosynthetic plastids where thioredoxins are held to play a central role in redox regulation.[29] Although a number of genes encoding either thioredoxin (Trx), putative Trxs or Trx-related proteins, and one encoding a Trx-reductase (TrxR), are present in *P. falciparum* genome, none has been described so far to be targeted to the apicoplast.[30] In a recent publication, Nickel *et al.*[31] suggested that two *P. falciparum* proteins (Trx2 and Trx3) are presumably apicoplast-resident thioredoxins, based on the detection of a predicted signal peptide at the N-terminus. However, *in vivo* targeting experiments are needed since such conclusion is not supported by other prediction algorithms (see http://v4-4.plasmodb.org/restricted/PlasmoAPcgi.shtml).

Apicoplast-resident thioredoxins would also require a thioredoxin reductase, but the single essential TrxR in *P. falciparum* is cytosolic. Therefore, alternative redox regulators should be sought to prevent PfFNR dimerization *in vivo*. One attractive possibility would be the involvement of lipoic acid (LA). Lipoate and dihydrolipoate constitute a strong redox couple (E_o = -290 mV), and LA is synthesized in the apicoplast.[32,33] Here, they exist as the protein-bound form in the E2 subunit of the apicoplast-resident pyruvate dehydrogenase complex[34], and probably to some extent also as lipoyl-containing small peptides or lipoyl-lysine, due to normal protein-turnover. Free, unbound LA is presumably not present in the apicoplast[35] however, it has

been shown that protein-bound LA may interact with external disulfides in its vicinity, including thioredoxins.[36]

CONCLUSIONS

The first crystal structures of an apicomplexan FNR reveal structural properties that are unique to plasmodial FNRs. Besides the extensive loop flexibility observed in two independent crystal structures and the new dimerization mechanism based on the oxidation of residue Cys99 in two opposing PfFNR subunits, a helix-coil transition has been shown to occur in the substrate (*i.e.*, $NADP^+$) binding region, where the 2'P-AMP inhibitor is bound. The occurrence of specific residues, unique of the plasmodial enzyme, that support such a conformational transition, renders this region of the PfFNR protein structure very attractive for the development of antimalarial compounds.

MATERIALS AND METHODS

NADH, $NADP^+$, NADPH, 2'P-AMP and $K_3Fe(CN)_6$ were purchased from Sigma; all other chemicals were of the highest grade, and used without further purification. Recombinant PfFNR was expressed and purified as described previously.[13]

Spectral Analyses – Absorption spectra were recorded either on an Agilent 8453 diode-array, or a Cary 100 double-beam (Varian) spectrophotometer. The PfFNR extinction coefficient (for the protein-bound flavin) was determined spectrophotometrically.[37] Steady-state kinetic parameters were determined for the NAD(P)H-$K_3Fe(CN)_6$ reductase, and the NADPH-INT reductase activities, as previously described.[10,20] The concentrations of both, the electron donor and the electron acceptor, were independently varied. Initial rate data were fitted to the equation for a ping-pong Bi-Bi mechanism by non-linear regression using the GraFit 5.0 software package (Erithacus Software Ltd., United Kingdom).

Molecular characterization methods – SDS-PAGE was carried out on 12% polyacrylamide gels. Analytical gel-filtration analyses were performed on an ÄKTA FPLC apparatus equipped with a Superdex 75 HR 10/30 column, equilibrated in 20 mM Tris-HCl, pH 7.4, containing 100 mM NaCl.

Active-Site Titrations – Titrations of PfFNR (15 μM) with either $NADP^+$, 2'P-AMP, and $K_3Fe(CN)_6$ were performed spectrophotometrically in 20 mM Tris-HCl, pH 7.6, at 16 °C using a Cary 100 (Varian) double-beam spectrophotometer. During titrations, spectra were recorded

initially and after additions of equal aliquots of ligand to the sample and reference cells. Difference spectra were computed by subtracting from each spectrum that obtained in the absence of ligand, after correction for dilution. K_d values were obtained by fitting data sets by nonlinear regression to the theoretical equation for a 1:1 binding.[38] Cys residues of PfFNR were titrated with DTNB (5,5'-dithiobis (2-nitrobenzoic acid)) under native conditions and after denaturation with 6 M guanidinium chloride, in 100 mM Na-phosphate, pH 7, containing 10% glycerol and 1 mM EDTA.[39]

Crystal growth and structure solution – PfFNR was co-crystallized with 2'P-AMP in batch setup under a 1:1 mix of paraffin and silicon oil, using an Oryx-6 crystallization robot (Douglas Instruments Ltd, UK). In particular, a 0.46 μl droplet containing the protein solution (28 mg/ml PfFNR, 10% glycerol, 50 mM Tris-HCl, pH 7.4, 1 mM DTT, 1 mM 2'P-AMP) was added to a 0.23 μl droplet containing the precipitant solution (22-25% PEG 4000, 0.1 M sodium cacodylate, pH 6.0, 0.2 M sodium acetate). The crystals grew in 2-3 weeks, at 294 K, as 150x150x50 μm^3. X-ray diffraction data were collected at 100 K (ESRF, Grenoble, beam line ID14-3) after 30 s of crystal soaking in a cryoprotectant solution (27% PEG 4000, 0.2 M sodium acetate, 0.1 M sodium cacodylate, pH 6, 26% glycerol). The data were indexed using the program Mosflm,[40] showing that the crystals belong to a primitive hexagonal space group, with unit cell parameters $a = b = 123.1$ Å, $c = 133.8$ Å. Scaling and merging of the data (to 2.7 Å resolution) using the program Scala[41] suggested two equally likely space groups: P3 (R_{merge} = 16.0%), or P321 (R_{merge} = 16.6%). The latter was chosen for the subsequent stages, based on the higher symmetry.

Molecular replacement searches, based on the Program Molrep[42] using as search model the structure of maize root FNR (pdb 16B9), allowed us to locate three FNR chains in the crystallographic asymmetric unit and assign the space group as $P3_121$ (V_M = 2.6 Å^3/Da, solvent content 52.5%). The corresponding R-factor and correlation coefficient values for the molecular replacement solution were 56.1% and 40.0%, respectively, for the data at 2.7 Å resolution, after rigid body refinement of the three independent protein chains. The protein model was subsequently refined using the program Refmac,[43] with a drop of the R_{gen}/R_{free} values to 28.1% / 33.9%, after several refinement cycles. At this stage clear electron density for an additional FNR molecule became evident in the crystallographic asymmetric unit. Such an observation, together with the occurrence of crystal packing intermolecular clashes, suggested to reduce the space group symmetry to $P3_1$. After rescaling of the data (resolution 2.7 Å, Rmerge = 10.2%), the well packed PfFNR dimer observed in the above refinement stages was used as search model, using Phaser,[44] now locating three PfFNR dimers in the crystallographic asymmetric unit. This model (6 independent PfFNR chains) was then refined using Refmac and modeled with O[45] (data at 2.7 Å resolution; R_{gen}/R_{free}= 24.3/31.7%). Each chain could be modeled in the 5–316 residue range, with the exclusion of the four regions 62-98, 126-133, 202-203 and 299-304, which displayed weak/absent electron density. Moreover, each subunit contained one FAD and one 2'P-AMP molecule (see Table 1). Additional crystallization experiments (using the same experimental setup) also yielded usable crystals at lower protein and inhibitor concentrations. In this case a 0.33 µl protein solution droplet (25 mg/ml PfFNR, 10% glycerol, 50 mM Tris-HCl, pH 7.4, 1 mM DTT, 0.5 mM 2'P-AMP, 0.2 mM Zinc acetate) was added to a 0.17 µl droplet containing the precipitant solution (22% PEG 4000, 0.1 M sodium citrate, pH 5.4, 0.2 M ammonium

acetate). Prismatic shaped crystals grew after 2-3 weeks at 291 K. Diffraction data were collected at ESRF beam line ID23-1, up to 2.4 Å resolution. Data reduction and scaling (programs Mosflm/Scala) showed that this crystal form belongs to the trigonal space group $P3_221$ (or enantiomorph), with unit cell parameters $a = b = 138.0$ Å $c = 147.4$ Å, accommodating four molecules in the crystal asymmetric unit (Matthews coefficient 2.7 $Å^3$/Da, solvent content 54.8%). The structure was solved by molecular replacement (program Phaser)[44] and refined using Refmac5 and manual rebuilding.[43,45] The four refined molecules (R_{gen}/R_{free}= 19.5/24.5%) display electron density for amino acids 5-316, with the exclusion of the regions 64-97, 126-133 and 197-202. The final refinement parameters are listed in Table 1.

Figures

Figures 3 and 4 were produced using CCP4mp.[46]

*Protein Data Bank Acsession code*s

Atomic coordinates and structure factors for both PfFNR and the PfFNR/2'P-AMP complex have been deposited with the Protein Data Bank, with entry codes …, ..., respectively.

ACKNOWLEDGMENTS

This work was supported by grants from Ministero dell'Istruzione, dell'Università e della Ricerca of Italy (Prin 2004) to GZ, and to MB (FIRB 2003 – Biologia Strutturale). MB is grateful to Fondazione Cariplo (Milano, Italy) and to CIMAINA (University of Milano) for continuous support.

REFERENCES

1. Maitland, K., Makanga, M. & Williams, T. N. (2004) Falciparum malaria: current therapeutic challenges. *Curr. Opin. Infect. Dis.* **17**, 405–412.

2. Gardner, M. J., Hall, N., Fung, E., White, O., Berriman, M., Hyman, R. W., Carlton, J. M., Pain, A., Nelson, K. E., Bowman, S., Paulsen, I. T., James, K., Eisen, J. A., Rutherford, K., Salzberg, S. L., Craig, A., Kyes, S., Chan, M.-S., Nene, V., Shallom, S. J., Suh, B., Peterson, J., Angiuoli, S., Pertea, M., Allen, J., Selengut, J., Haft, D., Mather, M. W., Vaidya, A. B., Martin, D. M. A., Fairlamb, A. H., Fraunholz, M. J., Roos, D. S., Ralph, S. A., McFadden, G. I., Cummings, L. M., Subramanian, G. M., Mungall, C., Venter, J. C., Carucci, D. J., Hoffman, S. L., Newbold, C., Davis, R. W., Fraser, C. M. & Barrell, B. (2002) Genome sequence of the human malaria parasite *Plasmodium falciparum*. *Nature* **419**, 498–511.

3. Foth, B. J. & McFadden, G. I. (2003) The apicoplast: a plastid in *Plasmodium falciparum* and other Apicomplexan parasites. *Int. Rev. Cytol.* **224**, 57–110.

4. Fichera, M. E. & Roos, D. S. (1997) A plastid organelle as a drug target in apicomplexan parasites. *Nature* **390**, 407–409.

5. He, C. Y., Shaw, M. K., Pletcher, C. H., Striepen, B., Tilney, L. G. & Roos D. S. (2001) A plastid segregation defect in the protozoan parasite *Toxoplasma gondii*. *EMBO J.* **20**, 330–339.

6. Ralph, S. A., van Dooren, G. G., Waller, R. F., Crawford, M. J., Fraunholz, M. J., Foth, B. J., Tonkin, C. J., Roos, D. S. & McFadden, G. I. (2004) Tropical infectious diseases: metabolic maps and functions of the *Plasmodium falciparum* apicoplast. *Nat. Rev. Microbiol.* **2**, 203–216.

7. Pink, R., Hudson, A., Mouries, M. A. & Bendig, M. (2005) Opportunities and challenges in antiparasitic drug discovery. *Nat. Rev. Drug Discov.* **4**, 727–740.

8. Seeber, F., Aliverti, A. & Zanetti, G. (2005) The plant-type ferredoxin-NADP$^+$ reductase/ferredoxin redox system as a possible drug target against apicomplexan human parasites. *Curr. Pharm. Des.* **11**, 3159–3172.

9. Vollmer, M., Thomsen, N., Wiek, S. & Seeber, F. (2001) Apicomplexan parasites possess distinct nuclear-encoded, but apicoplast-localized, plant-type ferredoxin-NADP$^+$ reductase and ferredoxin. *J. Biol. Chem.* **276**, 5483–5490.

10. Pandini, V., Caprini, G., Thomsen, N., Aliverti, A., Seeber, F. & Zanetti, G. (2002) Ferredoxin-NADP$^+$ reductase and ferredoxin of the protozoan parasite *Toxoplasma gondii* interact productively *in vitro* and *in vivo*. *J. Biol. Chem.* **277**, 48463–48471.

11. Thomsen-Zieger, N., Pandini, V., Caprini, G., Aliverti, A., Cramer, J., Selzer, P. M., Zanetti, G. & Seeber, F. (2004) A single in vivo-selected point mutation in the active center of *Toxoplasma gondii* ferredoxin-NADP$^+$ reductase leads to an inactive enzyme with greatly enhanced affinity for ferredoxin. *FEBS Lett.* **576**, 375–380.

12. Pandini, V., Caprini, G., Tedeschi, G., Seeber, F., Zanetti, G., & Aliverti, A. (2006) Roles of the species-specific subdomain and the N-terminal peptide of *Toxoplasma gondii* ferredoxin-NADP$^+$ reductase in ferredoxin binding. *Biochemistry* **45**, 3563–3571.

13. Röhrich, R. C., Englert, N., Troschke, K., Reichenberg, A., Hintz, M., Seeber, F., Balconi, E., Aliverti, A., Zanetti, G., Kohler, U., Pfeiffer, M., Beck, E., Jomaa, H. & Wiesner, J. (2005) Reconstitution of an apicoplast-localised electron transfer pathway involved in the isoprenoid biosynthesis of *Plasmodium falciparum*. *FEBS Lett.* **579**, 6433–6438.

14. Karplus, P. A. & Faber, H. R. (2004) Structural Aspects of plant ferredoxin: NADP$^+$ oxidoreductases. *Photosynth. Res.* **81**, 303–315.

15. Hanke, G. T., Kurisu, G., Kusunoki, M. & Hase, T. (2004) Fd:NFR electron transfer complexes: evolutionary refinement of structural interactions. *Photosynth. Res.* **81**, 317–327.

16. Hurley, J. K., Morales, R., Martinez-Julvez, M., Brodie, T. B., Medina, M., Gomez-Moreno, C. & Tollin, G. (2002) Structure-function relationships in *Anabaena* ferredoxin/ferredoxin:$NADP^+$ reductase electron transfer: insights from site-directed mutagenesis, transient absorption spectroscopy and X-ray crystallography. *Biochim. Biophys. Acta.* **1554**, 5–21.

17. Carrillo, N. & Ceccarelli, E. A. (2003) Open questions in ferredoxin-$NADP^+$ reductase catalytic mechanism. *Eur. J. Biochem.* **270**, 1900–1915.

18. Pandini, V., Caprini, G., Aliverti, A. & Zanetti, G. (2002) The plant-type ferredoxin-$NADP^+$ reductase of the protozoan parasite Toxoplasma gondii. In *Flavins and Flavoprotein 2002* (Chapman, S., Perham, R. & Scrutton, N., eds), pp.899–904.

19. Aliverti, A., Bruns, C. M., Pandini, V. E., Karplus, P. A., Vanoni, M. A., Curti, B. & Zanetti, G. (1995) Involvement of serine 96 in the catalytic mechanism of ferredoxin-$NADP^+$ reductase: structure--function relationship as studied by site-directed mutagenesis and X-ray crystallography. *Biochemistry* **34,** 8371–8379.

20. Aliverti, A., Piubelli, L., Zanetti, G., Lubberstedt, T., Herrmann, R. G. & Curti, B. (1993) The role of cysteine residues of spinach ferredoxin-$NADP^+$ reductase as assessed by site-directed mutagenesis. *Biochemistry* **32**, 6374–6380.

21. Batie, C. J & Kamin, H. (1986) Association of ferredoxin-$NADP^+$ reductase with NADP(H) specificity and oxidation-reduction properties. *J. Biol. Chem.* **261**, 11214–11223.

22. Bruns, C. M. & Karplus, P. A. (1995) Refined crystal structure of spinach ferredoxin reductase at 1.7 A resolution: oxidized, reduced and 2'-phospho-5'-AMP bound states. *J. Mol. Biol.* **247**, 125–145.

23. Bednarek, A., Wiek, S., Lingelbach, K. & Seeber, F. (2003) *Toxoplasma gondii*: analysis of the active site insertion of its ferredoxin-NADP(+)-reductase by peptide-specific antibodies and homology-based modeling. *Exp. Parasitol.* **103**, 68–77.

24. Karplus, P. A., Daniels, M. J. & Herriott, J. R. (1991) Atomic structure of ferredoxin-$NADP^+$ reductase: prototype for a structurally novel flavoenzyme family. *Science* **251**, 60–66.

25. Aliverti, A., Lubberstedt, T., Zanetti, G., Herrmann, R. G. & Curti, B. (1991) Probing the role of lysine 116 and lysine 244 in the spinach ferredoxin-$NADP^+$ reductase by site-directed mutagenesis. *J. Biol. Chem.* **266**, 17760–17763.

26. Medina, M., Luquita, A., Tejero, J., Hermoso, J., Mayoral, T., Sanz-Aparicio, J., Grever, K. & Gomez-Moreno, C. (2001) Probing the determinants of coenzyme specificity in ferredoxin-$NADP^+$ reductase by site-directed mutagenesis. *J. Biol. Chem.* **276**, 11902–11912.

27. Tejero, J., Martinez-Julvez, M., Mayoral, T., Luquita, A., Sanz-Aparicio, J., Hermoso, J. A., Hurley, J. K., Tollin, G., Gomez-Moreno, C. & Medina, M. (2003) Involvement of the pyrophosphate and the 2'-phosphate binding regions of ferredoxin-$NADP^+$ reductase in coenzyme specificity. *J. Biol. Chem.* **278**, 49203–49214.

28. Hermoso, J. A., Mayoral, T., Faro, M., Gomez-Moreno, C., Sanz-Aparicio, J. & Medina, M. (2002) Mechanism of coenzyme recognition and binding revealed by crystal structure analysis of ferredoxin-$NADP^+$ reductase complexed with $NADP^+$. *J. Mol. Biol.* **319**, 1133–1142.

29. Balmer, Y., Vensel, W. H., Cai, N., Manieri, W., Schurmann, P., Hurkman, W. J. &

Buchanan, B. B. (2006) A complete ferredoxin/thioredoxin system regulates fundamental processes in amyloplasts. *Proc. Natl. Acad. Sci. USA* **103**, 2988–2993.

30. Müller, S. (2004) Redox and antioxidant systems of the malaria parasite *Plasmodium falciparum*. *Mol. Microbiol.* **53**, 1291–1305.

31. Nickel, C., Rahlfs, S., Deponte, M., Koncarevic, S. & Becker, K. (2006) Thioredoxin networks in the malarial parasite *Plasmodium falciparum*. *Antioxid. Redox Signal.* **8**, 1227–1239.

32. Thomsen-Zieger, N., Schachtner, J. & Seeber, F. (2003) Apicomplexan parasites contain a single lipoic acid synthase located in the plastid. *FEBS Lett.* 547, 80–86.

33. Wrenger, C. & Müller, S. (2004) The human malaria parasite *Plasmodium falciparum* has distinct organelle-specific lipoylation pathways. *Mol. Microbiol.* **53**, 103–113.

34. Foth, B. J., Stimmler, L. M., Handman, E., Crabb, B. S., Hodder, A. N. & McFadden, G. I. (2005) The malaria parasite *Plasmodium falciparum* has only one pyruvate dehydrogenase complex, which is located in the apicoplast. *Mol. Microbiol.* **55**, 39–53.

35. Crawford, M. J., Thomsen-Zieger, N., Ray, M., Schachtner, J., Roos, D. S. & Seeber, F. (2006) *Toxoplasma gondii* scavenges host-derived lipoic acid despite its de novo synthesis in the apicoplast. *EMBO J.* **25**, 3214–3222.

36. Bunik, V. I. (2003) 2-Oxo acid dehydrogenase complexes in redox regulation. *Eur. J. Biochem.* **270**, 1036–1042.

37. Aliverti, A., Curti, B. & Vanoni, M. A. (1999) Identifying and quantitating FAD and FMN in simple and in iron-sulfur-containing flavoproteins. *Methods Mol. Biol.* **131**, 9–23.

38. Wang, Z. X., Kumar, N. R. & Srivastava, D. K. (1992) A novel spectroscopic titration method for determining the dissociation constant and stoichiometry of protein-ligand complex.

Anal. Biochem. **206**, 376–381.

39. Ellman, G. L. (1959) Tissue sulfhydryl groups. *Arch. Biochem. Biophys.* **82**, 70–77.

40. Leslie, A.G.W. 1992. Recent changes to the MOSFLM package for processing film and image plate data. Joint CCP4 and ESF-EACBM Newsletter 26.

41. Evans, P. R. (1997) Scaling of MAD data. In Proceedings of the CCP4 Study Weekend, Recent advances in phasing. Wilson, K.S., Davies, G., Ashton, A.W. & Bailey, S. Editors (CCLRC Daresbury Laboratory, Warrington), 97-102.

42. Vagin, A. & Teplyakov, A. 1997. MOLREP: an automated program for molecular replacement. *J. Appl. Cryst.* **30:** 1022-1025.

43. Murshudov, G. N., Vagin, A. A. & Dodson, E. J. (1997) Refinement of macromolecular structures by the maximum-likelihood method. *Acta Crystallogr. D* **53,** 240–255.

44. McCoy, A. J., Grosse-Kunstleve, R. W., Storoni, L. C. & Read, R. J. (2005) Likelihood-enhanced fast translation functions. *Acta Crystallogr. D* **61,** 458–464.

45. Jones, T. A., Zou, J. Y., Cowan, S. W. & Kjeldgaard, M. (1991) Improved methods for building protein models in electron density maps and the location of errors in these models. *Acta Crystallogr. A* **47,** 110–119.

46. Potterton, L., McNicholas, S., Krissinel, E., Gruber, J., Cowtan, K., Emsley, P., Murshudov, G. N., Cohen, S., Perrakis, A. & Noble, M. (2004) Developments in the CCP4 molecular-graphics project. *Acta Cryst. D* **60**, 2288–2294.

FIGURE CAPTIONS

Fig. 1. Formation of the disulfide-linked homodimeric form of PfFNR in solution. 300 μM PfFNR was incubated in the absence or in the presence of ligands at 20 °C in 50 mM Tris-HCl, pH 7.4, containing 10% glycerol. 8 μl aliquots were assayed by gel filtration on a Superdex 75 HR 10/30 column in 20 mM Tris-HCl, pH 7.4, containing 100 mM NaCl, after different incubation times: thin solid line, 1 h; dotted line, 1 day; thick solid line, 4 days; dashed line, 7 days. *A*, no ligand; *B*, 1 mM 2'P-AMP; *C*, 1 mM $NADP^+$.

Fig. 2. Binding of various ligands to PfFNR as studied by difference spectrophotometry. All enzyme titrations were carried out in 50 mM Tris-HCl, pH 7.6 at 16 °C. *A*, difference extinction coefficient of the binary complexes between PfFNR and 2'P-AMP (dashed line), $NADP^+$ (thin solid line) or $K_3Fe(CN)_6$ (thick solid line). *B*, titration with $K_3Fe(CN)_6$ of 20.4 μM PfFNR in the presence of 116 μM $NADP^+$. The reported spectra were recorded in the presence of the following concentration of ferricyanide: 0 (thin solid line), 50 μM (dotted line), and 470 μM (thick solid line). Intermediate titration spectra were omitted for clarity.

Fig. 3. Tertiary/quaternary structures in PfFNR and its 2'P-AMP complex. (A) the structure of one isolated chain of PfFNR (inhibitor-free, yellow ribbon) is overlaid on the structure of PfFNR/2'P-AMP (blue ribbon). The bound FAD (left) and 2'P-AMP (right) molecules are displayed as stick models. The lower right part of Panel A highlights the conformational helix-coil transition occurring at the β9-αF loop, in the $NADP^+$ domain, in the absence of the

nucleotide. (B) (drawn in the same orientation of Panel A) shows the PfFNR/2'P-AMP polypeptide chain (monomer), color coded for the atomic B-factors; red shows the highest temperature factors (B=60 $Å^2$), blue the lowest (B=10 $Å^2$). The FAD domain is on the left and the $NADP^+$ binding domain on the right. FAD and 2'P-AMP are displayed as cyan/red stick models. Note several interrupted segments on the protein surface, corresponding to regions of poor electron density. (C) View of the quaternary assembly observed in the crystal asymmetric unit of PfFNR. The four protein chains are shown in yellow, violet, orange and green, respectively, displaying their respective FAD bound species as stick models. (D) View of the dimeric assembly observed for the disulfide-stabilized PfFNR. The two protein chains are shown in yellow and green, respectively, displaying their respective FAD bound species as stick models. The yellow PfFNR subunit has the same orientation adopted in Panels A and B (two FAD groups are on the left hand side). The Cys99 disulfide, drawn in yellow, is labelled within a square window. (E) Stereo view of the covalent PfFNR/2'P-AMP dimer. The two PfFNR molecules are shown in blue and orange, respectively. The Cys99 disulfide is highlighted by a square box, and labelled. Two FAD molecules are shown as yellow stick models; 2'P-AMP stick models are in cyan. The blue subunit has the same orientation of the protein chain in Panels A and B.

Fig. 4. Electrostatics at the PfFNR $NADP^+$ binding site. (A) shows a mono view of the enzyme surface, colour coded for the distribution of electrostatic charges, around the 2'P-AMP (the lower green stick model in the figure; the 2' and 5' phosphate groups are labelled), and the FAD binding sites (the overall orientation of the protein is close to that of Figs. 3 A,B). A lack of

positive charge around the 2' phosphate group is evident, if just one PfFNR/2'P-AMP subunit is considered, as in this figure.

(B) when the PfFNR/2'P-AMP dimer is assembled, the electrostatic contribution of residues provided by the opposing subunit becomes evident around the 2' phosphate group of the inhibitor, as shown by the wider distribution of positive electrostatic charge (blue colour). Part of the secondary structure building the $NADP^+$ binding domain is shown as cyan ribbons. (colour code: red =-10 kT/e, white=0 kT/e, blue=10kT/e).

Fig. 5. Multiple sequence alignment of PfFNR, SoFNR, ZmFNR and TgFNR limited to the $NADP^+$ and 2'P-AMP recognition residues. The secondary structure elements (H, for α-helix; E, for β-strand) detected in the two crystal structures here reported are displayed in the lower lines. The sequence numbering is referred to SoFNR (above) and PfFNR (below). The highlighted residues are those interacting with the 2'P of NADP.

Table 1. Data collection and refinement statistics for PfFNR and its complex with 2'P-AMP

Data collection Statistics	PfFNR	PfFNR-2'P-AMP
Resolution [Å]	92.90 -2.40	61.60 - 2.70
Space group	$P3_221$	$P3_1$
Mosaicity [°]	0.4	0.7
Rmerge [%]	8.1 (48.9)[#]	10.2 (47.6)[*]
Total Observations	207307 (30565)	165850 (24078)
Unique Observations	63426 (9180)	61398 (8933)
Mean(I)/sd(I)	10.3 (2.9)	9.8 (2.3)
Completeness [%]	99.5 (99.7)	98.5 (98.1)
Multiplicity	3.3 (3.3)	2.7 (2.7)
Refinement Statistics		
R/Rfree [%]	19.5/24.5	24.3/31.7
R.M.S. Bond lengths [Å]	0.010	0.008
R.M.S. Bond angles [°]	1.30	1.27
Ramachandran Plot:		
Resid. in most fav. reg. [%]	91.3	88.4
Resid. in add. allow. reg. [%]	8.6	11.6

[*]High resolution shell: 2.85-2.70 Å

[#]High resolution shell: 2.53-2.40 Å

Table 2. Kinetic parameters of PfFNR

REACTION	k_{cat} ($e^-eq\ s^{-1}$)	$K_m^{NAD(P)H}$ (μM)	$k_{cat}/K_m^{NAD(P)H}$ ($s^{-1}\mu M^{-1}$)	$K_m^{acceptor}$ (μM)	$k_{cat}/K_m^{acceptor}$ ($s^{-1}\mu M^{-1}$)	K_i^{FeCN} (μM)
NADPH→$K_3Fe(CN)_6$[a]	250 ± 7.7	36 ± 5.7	7 ± 1	/	/	230 ± 40
NADH→$K_3Fe(CN)_6$[a]	96 ± 4	720 ± 90	0.1 ± 0.01	/	/	185 ± 22
NADPH→INT[b]	180 ± 11	350 ± 30	0.5 ± 0.05	95 ± 9	2 ± 0.2	/

[a]Activity was assayed at 25 °C in 100 mM Tris-HCl, pH 8.2

[b]Activity was assayed at 25 °C in 200 mM Tris-HCl, pH 9.0, containing 70 mM NaCl and 0.1% Triton-X100

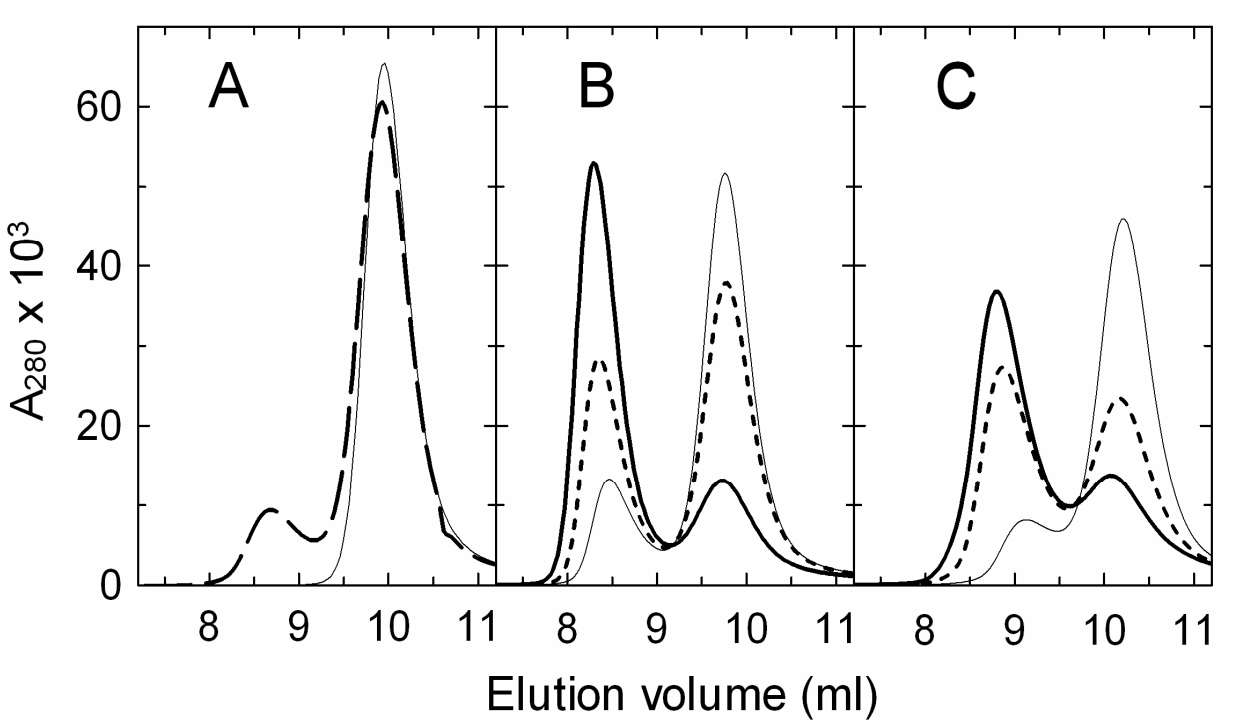

Fig. 1

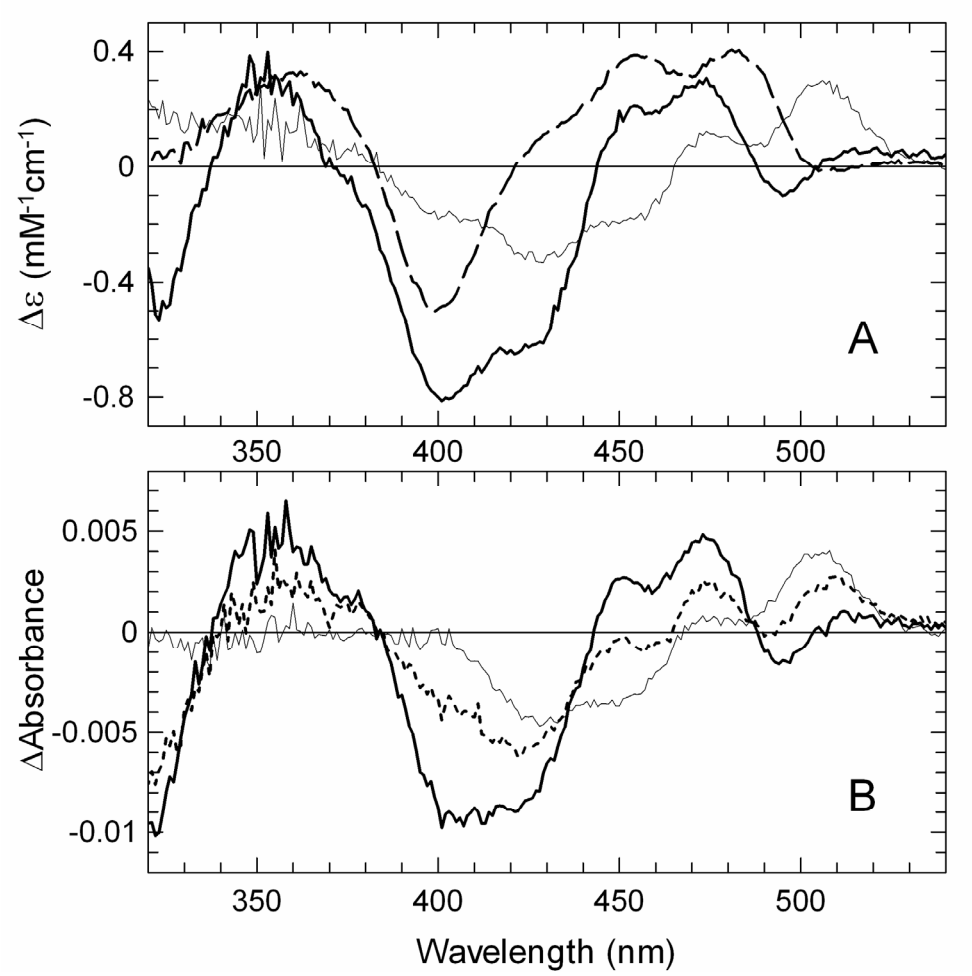
0.4
0
-0.4
-0.8
Δε (mM-1cm-1)
A
350
400
450
500
0.005
0
-0.005
-0.01
ΔAbsorbance
B
350
400
450
500
Wavelength (nm)

Fig. 2

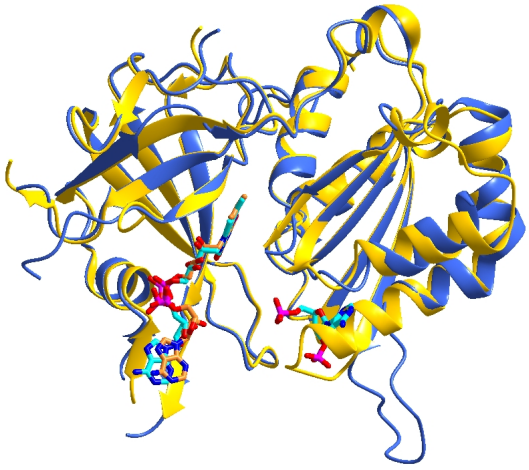

A

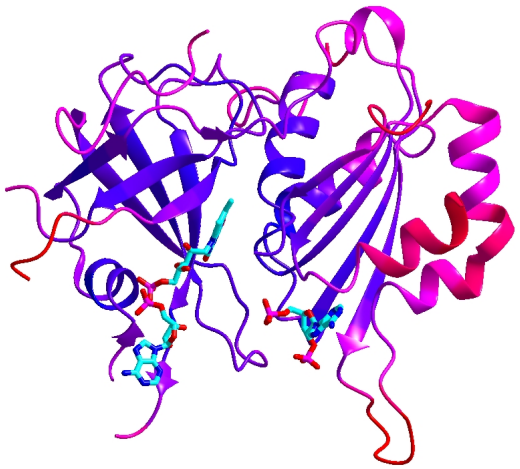

B

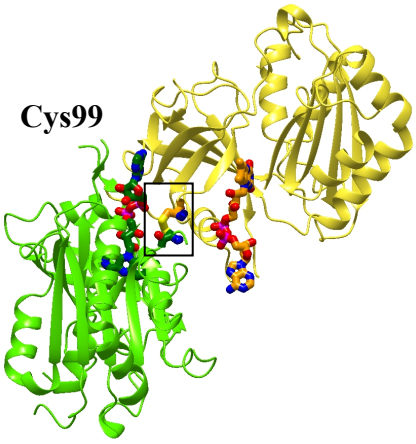

C

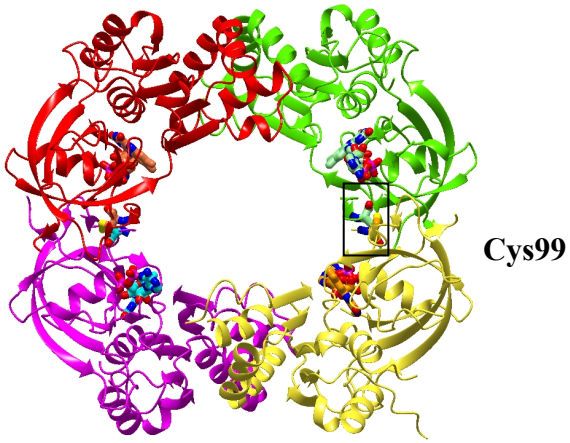

D

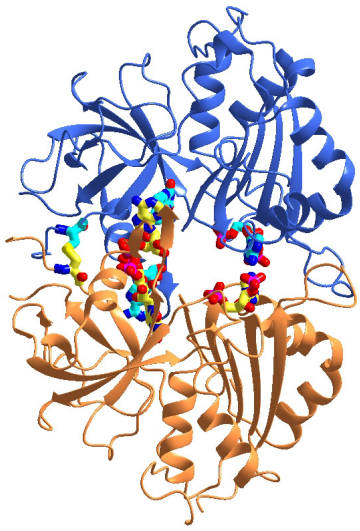

D

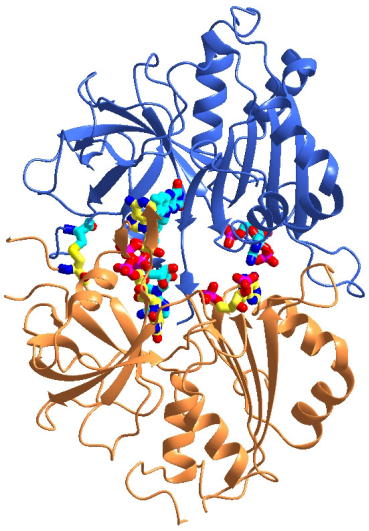

Fig.3

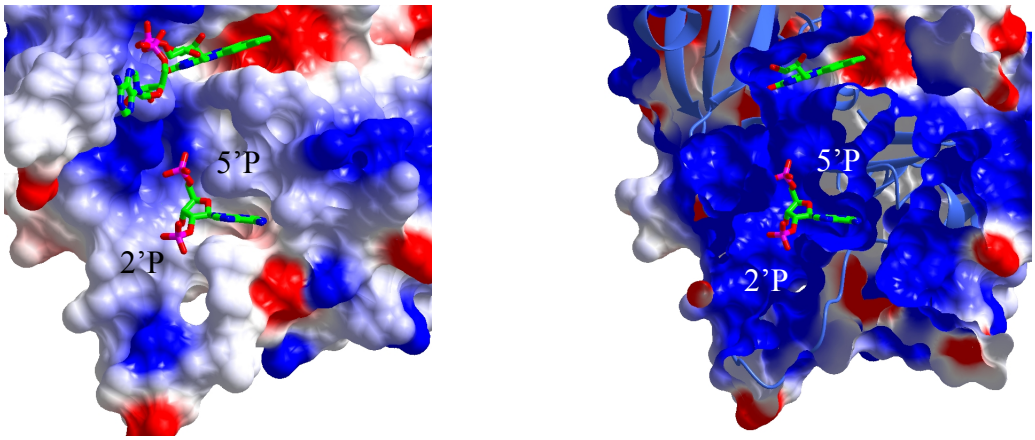

A **B**

Fig. 4

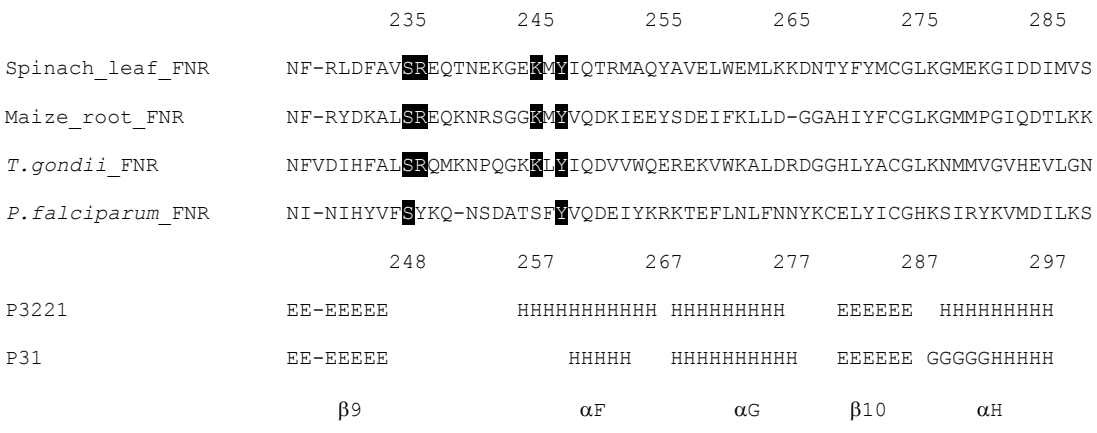
235 245 255 265 275 285
Spinach_leaf_FNR NF-RLDFAVSREQTNEKGEKMYIQTRMAQYAVELWEMLKKDNTYFYMCGLKGMEKGIDDIMVS
Maize_root_FNR NF-RYDKALSREQKNRSGGKMYVQDKIEEYSDEIFKLLD-GGAHIYFCGLKGMMPGIQDTLKK
T.gondii_FNR NFVDIHFALSRQMKNPQGKKLYIQDVVWQEREKVWKALDRDGGHLYACGLKNMMVGVHEVLGN
P.falciparum_FNR NI-NIHYVFSYKQ-NSDATSFYVQDEIYKRKTEFLNLFNNYKCELYICGHKSIRYKVMDILKS
248 257 267 277 287 297
P3221 EE-EEEEE HHHHHHHHHHH HHHHHHHHH EEEEEE HHHHHHHHH
P31 EE-EEEEE HHHHH HHHHHHHHHH EEEEEE GGGGGHHHHH
β9 αF αG β10 αH

Fig. 5